Proceedings of the IASS 2024 Symposium
Redefining the Art of Structural Design
August 26-30, 2024, Zurich Switzerland
Philippe Block, Giulia Boller, Catherine DeWolf,
Jacqueline Pauli, Walter Kaufmann (eds.)

Research on Mechanical Properties of Hot-dip galvanized Large Hexagonal Head High Strength Bolt

Liu Dong*, Yu Xianglin*, Zhao Shihua*, Shi Yongjiu*, Wen JiangTao[a], Zhang Shuang[a], Shi Jun[a]

* Department of Civil Engineering, Tsinghua University, Beijing 100084, China
1065129737@qq.com

[a] China Construction Third Engineering Bureau Group Co., Ltd., Wuhan 430205, China

Abstract

As a critical joint component, the high-strength (HS) bolt is extensively used in various types of structures. Based on the 276 m high-rise pure steel TV tower being constructed in the windy and corrosion-prone region of Northwest China, various specifications of Grade 8.8 HS bolts are applied in this structure. Under this circumstance, two specifications of HS bolts with large hexagon head and large diameter are investigated via uniaxial tensile experiment. Besides, the impact of different sampling positions and surface treatment methods (with or without hot-dip galvanizing) on the mechanical properties is also taken into account. Typical mechanical properties, stress-strain curves, bolt pre-tensions and tightening torques for the HS bolts with large diameter are obtained from the experiment. In general, test results indicate that hot-dip galvanizing and different sampling positions have limited impact on the mechanical performance of HS bolts. Furthermore, according to the measured stress-strain curves and critical mechanical indicators, a reasonable full-range stress-strain constitutive model is proposed and made detailed comparisons with existing constitutive models, which shows sufficient accuracy (as high as 99.86% goodness of fit) for HS bolts. Therefore, the proposed constitutive model can be used to simulate the stress-strain relationship in the design and numerical modelling of HS bolts with large hexagon head and large diameter.

Keywords: Steel structures, mechanical properties, stress-strain constitutive model, high-strength bolt, large diameter, uniaxial tensile test, hot-galvanizing, pre-tension.

1. Introduction

Large-diameter high-strength bolts play a pivotal role in high-performance building structures, frequently used in large-diameter flange tubular joints and large-sized gusset plate connections. The study of the mechanical properties, constitutive relationships, and preload design of high-strength bolts in key connections is particularly important. The primary performance indicators of bolts are detailedly studied, including tensile behavior [1-5], shear behavior [6-9], tensile-shear behavior [10, 11], fatigue performance [12], corrosion resistance [13-16], impact toughness [17], pre-tension [6, 18, 19] and preload losses [20, 21], etc. Besides, the mechanical properties of HS bolts under- and post- fire [22-28] are studied and relevant formulas regarding the reduction factors and constitutive models are proposed. Previous literatures regarding the properties of HS bolts are primarily based on regular diameter (not exceeding 30 mm) specified in existing standards, thus whether the related conclusions are equivalently applicable to large-diameter HS bolts or not, still needs to be ascertained and deserves further investigation. As one of a series of scientific research aiming at the 276m pure steel TV tower constructed in Yinchuan (see Fig. 1), Northwest China, comparative experimental investigations are carried out on the mechanical properties of large-diameter and large-hexagon head Grade 8.8 HS bolts used in flange or gusset plate connections under hot-dip zinc protection (see Fig. 2), so as to determine

the mechanical performance indicators of hot-dip galvanized HS bolts, as well as the pre-tension value and tightening torque.

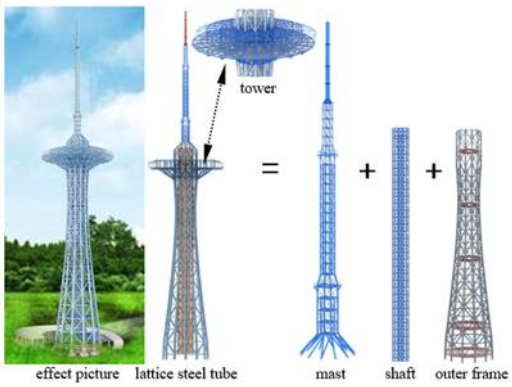

Figure 1: Overview of Yinchuan TV Tower

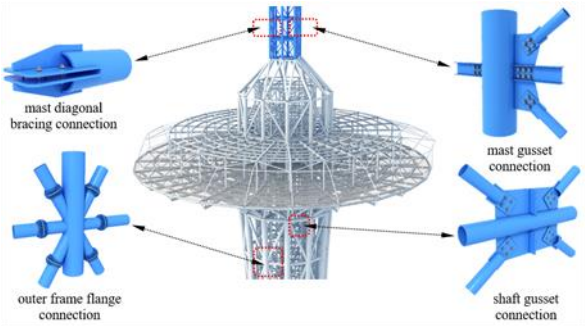

Figure 2: Applications of large-diameter bolt connections

Based on the experimental stress-strain curves and existing constitutive models, a full-range stress-strain constitutive model suitable for HS bolts with large diameter and large hexagon head is proposed. Nonlinear regression analysis and statistical analysis are performed on the model parameters to determine their intrinsic relationships, mathematical and physical implications, and influencing extents on the constitutive model. A deterministic constitutive model that characterizes the mechanical properties of each test specimen and related parametric values are obtained. The application of material property test results and proposed stress-strain constitutive models to the finite element modeling and numerical analysis, can provide a theoretical basis and calculation reference for further analyzing the stress distribution and deformation characteristics of the fully bolted connections in the TV tower structure.

2. Experimental program

2.1. Test specimen design

Based on a 276 m high-rise steel TV tower in progress, the Grade 8.8 HS large hexagon-head and large diameter bolts are extensively used with many specifications, including M36×150, M42×170, M48×180 and M52×190, among which the mechanical properties and full-range stress-strain relationships for M36×150 and M48×180 bolts are subjected to investigation. The chemical compositions of the two specifications of HS bolts are summarized in Table 1, both meeting the requirements of the relevant standard [30]. In the practical high-rise television tower structure located at the northwest China, all adopted bolts are hot-dip galvanized so as to solve the issues of bolt corrosion and durability under extremely complex climatic circumstances. Considering that the bolt surface temperature is normally above 420℃ during the hot-dip galvanizing process and the Grade 8.8 HS bolts are conventionally manufacured from HS alloy steels, the metallographic structure of the hot-galvanized bolts might be sensitive to high temperatures and take substantial transformation of the microstructure, which might engender remarkable impact on the fundamental mechanical properties and pre-tensions. For this reason, uniaxial tensile tests are carried out with respect to the two specifications of HS bolts (M36 × 150 and M48 × 180), hot-dip galvanized (MG) and non hot-dip galvanized (M), which have been used in the current construction process (tower height below 50 meters). In addition, the material properties of HS hot-dip galvanized bolts and screws at different positions may vary significantly due to the influence of high temperature, thus the sampling positions are different. Sampling and experimental comparative studies were conducted on the material mechanical properties under three different conditions: standard position (S) [31], bolt rod center (C), and bolt rod edge (E) (as shown in Fig. 3). All bolts (see Fig. 4) for test specimens are originated from the practical Yinchuan TV Tower. According to the results provided in the bolt Quality Inspection Report, the measured thickness of the hot-dip zinc coating is 77-89 μm (for M36 × 150) and 79-96 μm (for M48 × 180), meeting the requirement of the standard values specified in the code [32]. All tensile test specimens are standard proportional specimens sampled from

the screws. The diameter of the center section is 10 mm, and the original gauge length is 50 mm (i.e. 5.65). The threads of the gripping ends are processed according to the thread specifications of the M16 bolt. The specific dimensions and photo are shown in Fig. 5.

Table 1: Chemical compositions of Grade 8.8 HS large hexagon-head bolts and their sets (%)

specification	parts	value	C	Mn	Si	S	P	Cr
M36×150	screw	standard	0.37～0.44	0.50～0.80	0.17～0.37	≤0.030	≤0.030	0.80～1.10
		measured	0.39	0.60	0.22	0.005	0.012	0.88
	nut	standard	0.42～0.50	0.50～0.80	0.17～0.37	≤0.035	≤0.035	—
		measured	0.43	0.58	0.22	0.003	0.013	—
	washer	standard	0.42～0.50	0.50～0.80	0.17～0.37	≤0.035	≤0.035	—
		measured	0.48	0.66	0.24	0.008	0.013	—
M48×180	screw	standard	0.37～0.44	0.50～0.80	0.17～0.37	≤0.030	≤0.030	0.80～1.10
		measured	0.39	0.70	0.24	0.005	0.015	0.94
	nut	standard	0.42～0.50	0.50～0.80	0.17～0.37	≤0.035	≤0.035	—
		measured	0.46	0.58	0.24	0.004	0.019	—
	washer	standard	0.42～0.50	0.50～0.80	0.17～0.37	≤0.035	≤0.035	—
		measured	0.50	0.59	0.22	0.002	0.015	—

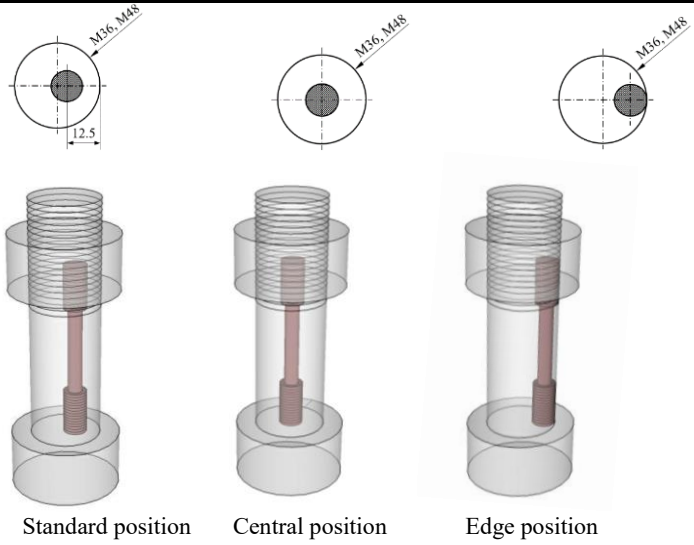

Figure 3: Sampling position of test specimen from the practical HS bolts with large hexagon head

Figure 4: Bolt specifications applied in Yinchuan TV tower

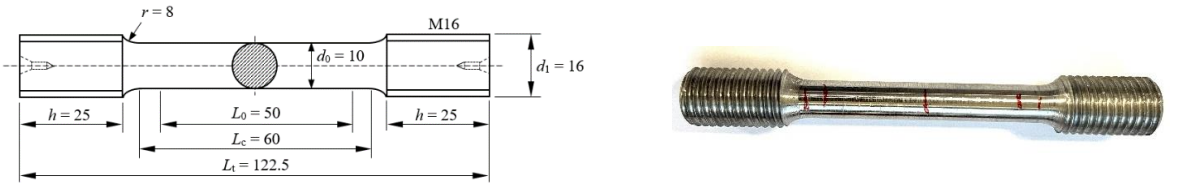

(a) (b)

Figure 5: Test specimen for bolt material properties: (a) dimensions; (b) photo

Table 2: Design values of standard tensile specimens processed from Grade 8.8 HS bolts(mm)

parameter	d_0	L_0	r	d_1	h	L_c	L_t
name	parallel diameter	original gauge length	transition arc radius	gripping diameter	gripping length	parallel length	total length
design value	10	50	8	16	25	60	122.5

The standard tensile specimens were processed with reference to GB/T 228.1-2021 [33] and ISO 6892-1 [34], and their nominal dimensions and measured values are shown in Tables 2 and 3. The measured results indicate that the deviation between the measured values of the geometric dimensions of the sample and the design values is small. For bolt specimens with the same specifications, sampling locations, and surface treatment methods, two identical tensile specimens are taken for tensile testing, as shown in Table 3.

Table 3: Measured dimensions of standard specimens processed from Grade 8.8 HS bolts (mm)

specimen	d_{0t} (mm)	d_{0m} (mm)	d_{0b} (mm)	d_0 (mm)	L_0 (mm)	S_0 (mm^2)	L_c (mm)	L_t (mm)
M36S-1	9.55	9.64	9.66	9.62	50.64	72.63	60.00	122.5
M36S-2	9.69	9.69	9.68	9.69	50.20	73.70	60.00	122.5
M36C-1	10.01	9.94	10.06	10.00	51.03	78.59	60.00	122.5
M36C-2	9.72	9.80	9.86	9.79	50.57	75.33	60.00	122.5
M36E-1	9.44	9.58	9.69	9.57	50.12	71.93	60.00	122.5
M36E-2	9.67	9.83	9.76	9.75	50.18	74.71	60.00	122.5
MG36S-1	9.71	9.73	9.78	9.74	50.61	74.51	60.00	122.5
MG36S-2	9.85	9.88	9.89	9.87	50.75	76.56	60.00	122.5
MG36C-1	9.51	9.83	9.97	9.77	49.64	74.97	60.00	122.5
MG36C-2	9.51	9.82	9.89	9.74	49.67	74.51	60.00	122.5
MG36E-1	10.00	10.05	9.97	10.01	50.41	78.64	60.00	122.5
MG36E-2	9.83	9.80	9.78	9.80	50.07	75.48	60.00	122.5
M48S-1	9.69	9.72	9.76	9.72	50.02	74.25	60.00	122.5
M48S-2	9.77	9.85	9.92	9.85	50.46	76.15	60.00	122.5
M48C-1	9.90	9.89	9.97	9.92	50.80	77.29	60.00	122.5
M48C-2	9.59	9.61	9.67	9.62	50.53	72.73	60.00	122.5
M48E-1	9.71	9.75	9.79	9.75	50.01	74.66	60.00	122.5
M48E-2	9.76	9.79	9.81	9.79	50.52	75.22	60.00	122.5
MG48S-1	9.75	9.79	9.85	9.80	50.57	75.38	60.00	122.5
MG48S-2	9.67	9.75	9.85	9.76	50.44	74.76	60.00	122.5
MG48C-1	10.14	9.85	10.04	10.01	50.39	78.70	60.00	122.5
MG48C-2	10.14	10.18	10.00	10.11	50.11	80.22	60.00	122.5
MG48E-1	10.01	9.94	10.06	10.00	51.03	78.59	60.00	122.5
MG48E-2	9.66	9.69	9.72	9.69	49.83	73.75	60.00	122.5

Note：M36S: 36 denotes that the nominal diameter of HS bolt is 36 mm, S denotes that the sampling position is standard position of screw; M36C-1: C denotes that the sampling position is central position of screw, -1 denotes the first parallel test specimen; M36E-1: E denotes that the sampling position is edge postion of screw; MG36C-1: G denotes that the test specimen is sampled from the hot-dip galvanized bolt; d_{0t}、d_{0m}、d_{0b} denote the diameters of the top, middle, bottom locations of the

original gauge range; d_0 denotes the average diameter of the original gauge range, taken as the average value of d_{0t}, d_{0m} and d_{0b}; S_0 denotes the average sectional area of the original gauge range, calculated by $S_0 = \pi d_0^2/4$.

2.2. Test setup

The tensile test of the mechanical properties of HS bolts was conducted on an electro-hydraulic servo universal testing machine in the Structural Laboratory of Tsinghua University. The maximum loading force of the testing machine is 500 kN, and the test setup is shown in Fig. 6. During the experiment, the gripping parts of the specimen are screwed into the sleeve, and then the tension and friction are applied to the sleeve, as shown in Fig. 7.

Figure 6: Uniaxial tensile test setup

Figure 7: Bolt specimen installation

Figure 8: Arrangement of extensometer and strain gauge

2.3. Standard test method

According to the standard tensile testing method specified in the national standard GB/T 228.1-2021 [33] and the international standard ISO 6892-1 [34], the mechanical properties of hot-dip galvanized and non hot-dip galvanized Grade 8.8 HS bolts were investigated via uniaxial tensile tests at room temperature. Because the test specimen exhibits favorable uniform deformation, in order to obtain a more accurate, continuous, and smooth stress-strain curve, a strain rate based on the feedback from the extensometer (Method A1 closed loop) [33] was used before removing the extensometer. The recommended strain rate of 0.00025s-1 in the standard was selected for loading, in order to obtain the proof strength at a specified plastic strain (Rp) and percentage yield point extension (Ae). When measuring the tensile strength (Rm), percentage elongation after fracture (A), and percentage reduction area (Z), the estimated strain rate over the parallel length is used, which is achieved by using the crosshead separation rate calculated by multiplying the required strain rate by the parallel length (Method A2 open loop) [33], and the recommended strain rate of 0.0067s-1 is selected for loading. The mechanical indicators are calculated according to the relevant formulas in the standards [33, 34].

2.4. Test observation

All test specimens exhibit continuous and uniform deformation characteristics during the axial tensile loading process, and noticeable necking phenomenon occurs on the verge of tensile fracture, as shown in Fig. 9(a). After the specimen shows tensile failure, the fracture section appears rough and uneven at the micro-level, but in general it is approximately perpendicular to the length direction (see Fig. 9(b)). The majority of specimens have fracture locations within the original gauge range, with only a few specimens experiencing fracture between the parallel and original gauge ranges. The typical failure characteristics of the specimens are shown in Fig. 9(c). The fracture morphology of all specimens is extremely similar as shown in Fig. 10, indicating that hot-dip galvanizing and sampling position have no significant effect on the fracture morphology of the specimens, but have a certain impact on the elongation after fracture.

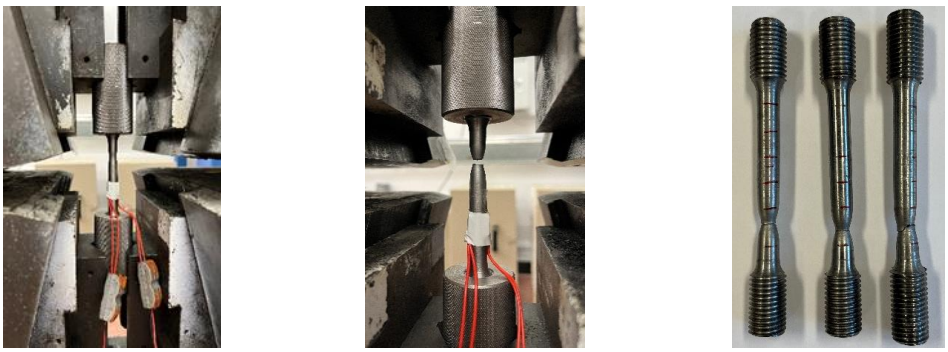

(a) (b) (c)

Figure 9: Test observation: (a) necking process; (b) after fracture; (c) typical fracture characteristics

Figure 10: Failure morphology of all test specimens

3. Experimental results and analyses

3.1. Experimental stress-strain curves

The measured full-range stress-strain curves of typical test specimens are shown in Fig. 11. It can be seen from the stress-strain curves that all specimens have no apparent yield plateau, thus their nominal yield strength can be characterized by the proof strength Rp0.2 at a specified 0.2% plastic strain. The full-range stress-strain curve can be divided into three stages: linear ascending stage, nonlinear hardening stage, and nonlinear necking stage. Besides, the elongation within the gauge length (50 mm) measured by the extensometer is generally between 5% and 15%. When the average strain within the gauge length reaches 5%, the axial tensile force is basically approximate to or reaches the ultimate tensile strength of the specimen. Therefore, it is reasonable to consider that the ultimate strains of all test specimens are around 5%. Based on the full-range stress-strain curve, fundamental mechanical indicators such as Young's modulus, proof strength, tensile strength, elongation after fracture, and percentage reduction area can be calculated.

3.2. Young's modulus

According to Appendix D [33] of the national standard GB/T 228.1-2021, the Young's modulus of bolt specimens can be obtained by regression analysis of the linear segment of the stress-strain curve in uniaxial tensile tests, as shown in Table 4 and Fig. 12. As shown in the figure, all the average Young's moduli of two identical specimens are between 200 GPa and 220 GPa, while the average Young's moduli of M36 (i.e. M36S+M36C+M36E), MG36 (i.e. MG36S+MG36C+MG36E), M48 (i.e. M48S+M48C+M48E), M48S, M(G)36 (i.e. M36+MG36), M(G)48 (i.e. M48+MG48), and all 24 test specimens are around 210 GPa. For MG36E specimens, the average Young's modulus is significantly lower than that without hot-dip galvanizing, indicating that the Young's modulus at the edge of the bolt is degraded due to the thermal influence of hot-dip galvanizing.

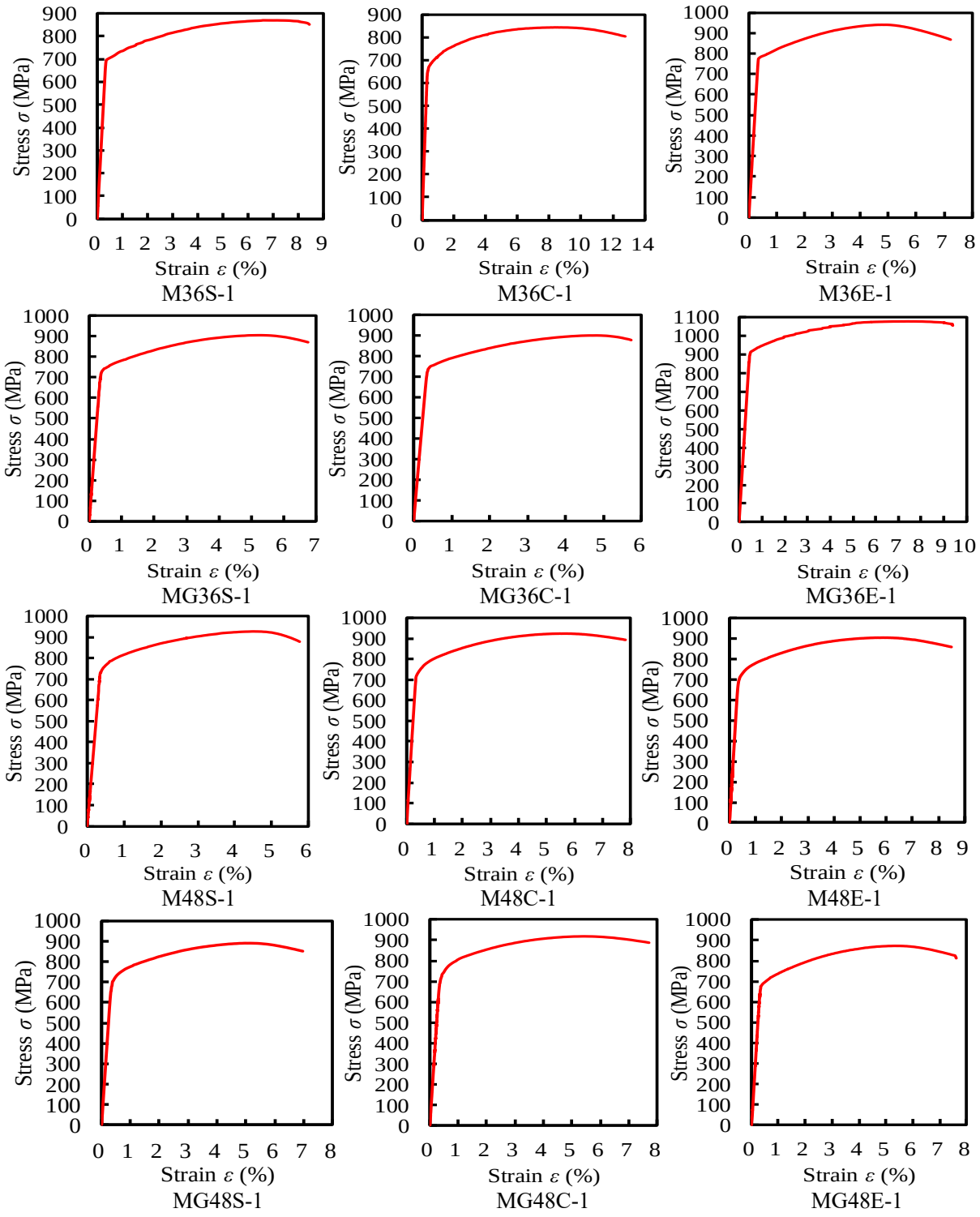

Figure 11: Typical measured full-range stress-strain curves

However, the MG48E specimens demonstrate the opposite case, which is unbelievable and deserves further study. The average Young's moduli of MG48S+MG48C specimens are also lower than their corresponding values of M48 specimens, while MG36S+MG36C specimens present the reverse case, indicating that the effect of hot-dip galvanizing on the Young's modulus at standard or center positions has no obvious pattern. Furthermore, for M36 and M48 specimens, the Young's moduli sampled at the edge of the screw are significantly higher than those sampled at the center or standard positions, and the Young's moduli of the latter are quite approximate, indicating that the farther the sampling position is

from the center of the bolt, the greater the Young's modulus. However, for MG36 specimens, the thermal effect significantly weakens the Young's modulus at the edge position, resulting in lower values than those at the center or standard positions, but MG48 specimens show the opposite effect. Therefore, the actioning mechanism of hot-dip galvanizing on the HS bolt is not ascertained. In addition, by comparing the test results obtained from specimens sampled at the standard position (see the numbers in parentheses in Table 4), it can be seen that except the sampling at the edge of M36 and MG36, the Young's moduli sampled at different positions have slight differences from the test results obtained from sampling at the standard position, but the difference is not significant (the deviations all within 3%).

Table 4: Measured Young's modulus of standard tensile specimens

sampling position	specimen	Young's modulus E_b (MPa)	mean value E_{bm} (MPa)	specimen	E_b (MPa)	E_{bm} (MPa)
standard position	M36S-1	206196	202893	M48S-1	208390	210028
	M36S-2	199590		M48S-2	211666	
	MG36S-1	209001	214323	MG48S-1	209428	208060
	MG36S-2	219645		MG48S-2	206691	
central position	M36C-1	199336	204088 (0.6%)	M48C-1	219668	209501 (-0.3%)
	M36C-2	208840		M48C-2	199333	
	MG36C-1	208698	210946 (-1.9%)	MG48C-1	209548	208260 (0.1%)
	MG36C-2	213193		MG48C-2	206971	
edge position	M36E-1	231782	220069 (8.5%)	M48E-1	214835	215494 (2.6%)
	M36E-2	208355		M48E-2	216153	
	MG36E-1	200066	202976 (-5.6%)	MG48E-1	212303	212532 (2.1%)
	MG36E-2	205886		MG48E-2	212761	

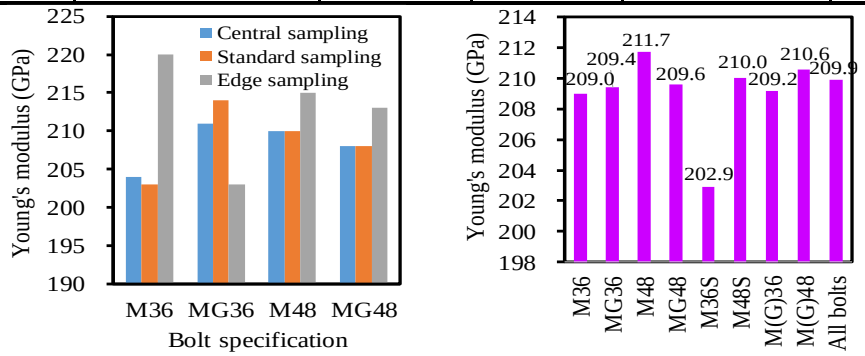

Figure 12: Comparison of measured Young's moduli for all test specimens.

3.3. Constitutive model for high-strength bolts

Existing stress-strain models applied to HS bolts are seriously inaccurate around the knee of the stress-strain curve, irrespective of Ramberg-Osgood model, Rasmussen model or Shi model. Based on the Shi model, a further modified full-range stress-strain model for HS bolts is proposed as follows:

$$\varepsilon = \begin{cases} \dfrac{\sigma}{E_{0b}} + \alpha\left(\dfrac{\sigma}{R_{p0.2}}\right)^{n}, & \text{for } \sigma \le R_{p0.2} \quad \text{Stage 1} \\ \varepsilon_{0.2} + \dfrac{\sigma - R_{p0.2}}{\chi E_{0.2b}} + \beta\left(\dfrac{\sigma - R_{p0.2}}{R_m - R_{p0.2}}\right)^{m}, & \text{for } R_{p0.2} < \sigma \le R_m \quad \text{Stage 2} \end{cases} \tag{1}$$

where E_{0b} is the initial Young's modulus for Grade 8.8 HS bolts; $R_{p0.2}$ is the 0.2% proof stress (equivalent to σ0.2); n and m are the strain hardening exponents; α and β are the regression parameters from experimental data; R_m is the ultimate tensile strength (equivalent to σu); $E_{0.2b}$ (equivalent to $E_{0.2}$) is the bolt initial tangent modulus of the stress-strain curve at $R_{p0.2}$; χ is the shape optimization factor for

improving the accuracy of the curve simulation at Stage 2, in view of the sharp change in slope around the knee region of the stress-strain curve (all experimental values of $E_{0.2b}/E_{0b}$ are less than 0.1, leading to n > 10).

By performing the nonlinear regression analysis of the strain hardening exponent n (which is based on the proposed model and test results) versus the stress ratio $R_{p0.01}/R_{p0.2}$ (from Table 10), the following expression is established:

$$n = \frac{2.972}{\mathrm{In}\left(R_{p0.2}/R_{p0.01}\right)} \approx \frac{\mathrm{In}(20)}{\mathrm{In}\left(R_{p0.2}/R_{p0.01}\right)} \tag{2}$$

As shown in Fig. 13, good agreement (with R_2 = 98.27) between the proposed constitutive model and the fitting curve is reached for Grade 8.8 HS bolts. Besides, the values of the strain hardening exponent n for M36 HS bolts are generally larger than those for M48 HS bolts, because the latter present lower stress ratio ($R_{p0.01}/R_{p0.2}$) than the former.

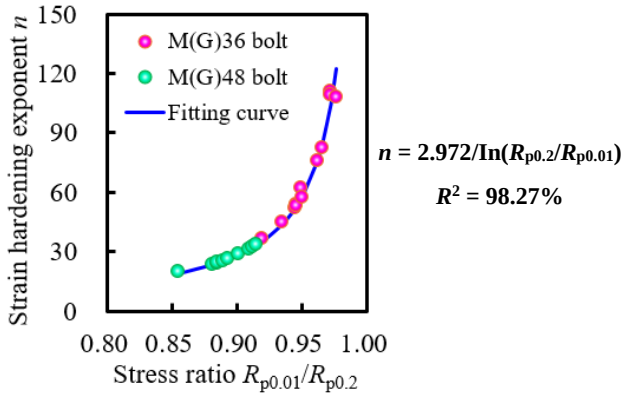

Figure 13: Relationship between n and $R_{p0.01}/R_{p0.2}$ for all test specimens

The relationship between the second-stage strain hardening exponent m and the yield ratio Rp0.2/Rm is plotted in Fig. 14(a). Apparently, the correlation between the two parameters is indistinct. Besides, the relationship between β and Rp0.2/Rm is also ambiguous (see Fig. 14(b)); however, if we define $\zeta = \varepsilon_u - \frac{R_m - R_{p0.2}}{\chi E_{0.2b}} - \varepsilon_{0.2}$, the correlation between β and ζ becomes very explicit with the coefficient of correlation at 97.55% and goodness of fit at 95.16% (see Fig. 14(c)).

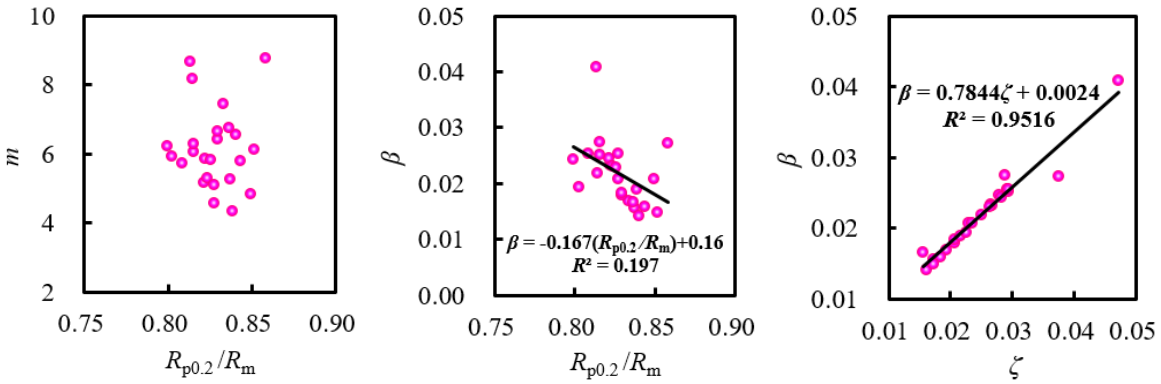

(a) m versus $R_{p0.2}/R_m$ (b) β versus $R_{p0.2}/R_m$ (c) β versus ζ

Figure 14: Relationships among the parameters of the proposed constitutive model

The influence of the regression parameters χ, β and m on the second-stage curve and on the goodness of fit of the proposed model for M36S-2 is shown in Fig. 15. Obviously, the exact values for the parameters corresponding to the optimal model are consistent with the values. In general, when χ, β and m take average values of 0.818, 0.022 and 6.171, the most accurate model for the second-stage expression of all tested HS bolts are obtained. With respect to the first-stage expression, the optimal value for the parameter α takes as 0.002.

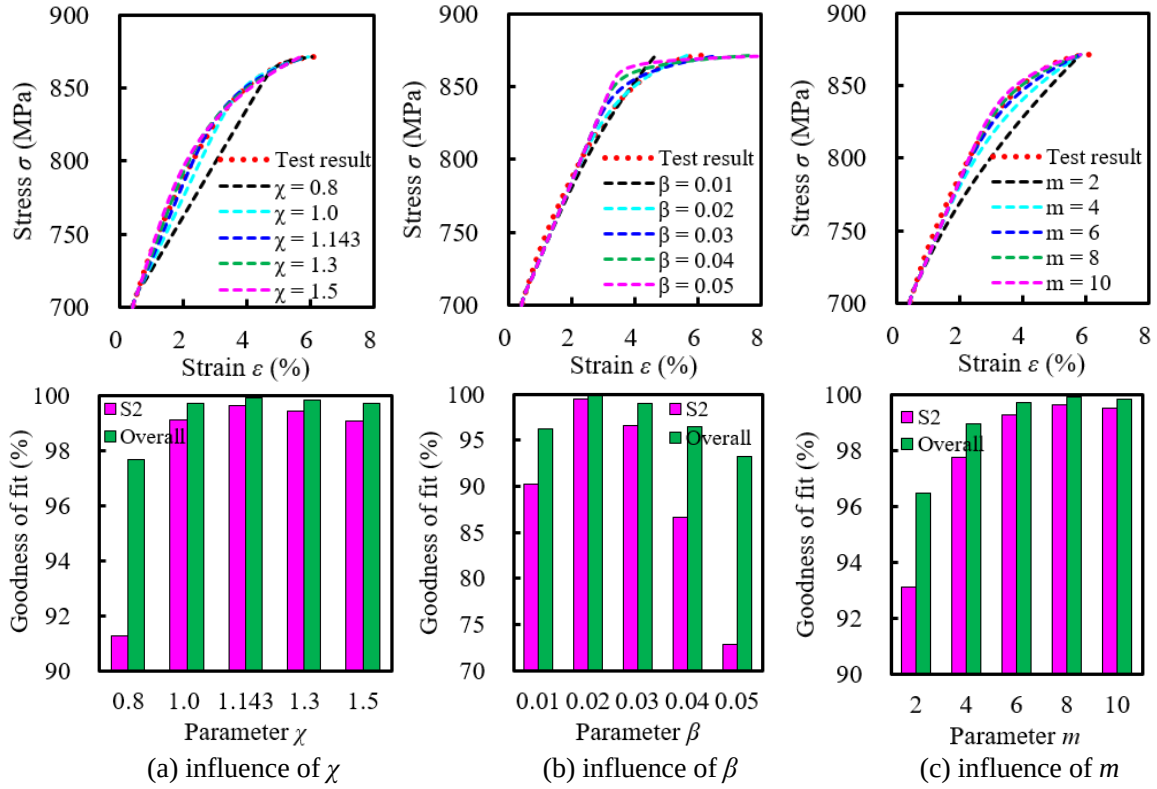

(a) influence of χ (b) influence of β (c) influence of m

Figure 15: The influence of parameters on the proposed constitutive model for M36S-2

4. Conclusion: submission of contributions

Uniaxial tensile tests on two specifications of large-diameter Grade 8.8 HS bolts with large hexagon head are carried out, in order to obtain the stress-strain curve and fundamental mechanical performance indicators. The influence of important factors such as different sampling positions and different surface treatment methods on mechanical properties is analyzed in depth. Based on the experimental results and standard calculation formulas, the pre-tensions and tightening torques for two different specifications of HS bolts are obtained. According to the experimental results and existing constitutive models in literatures, model parameter selection, optimization, and regression analysis are carried out to obtain a suitable full-range stress-strain constitutive model and recommended parameter values.

Acknowledgements

The authors gratefully acknowledge the support from the National Natural Science Foundation of China (Grant No. 52378163, 51890903). Sincere gratitudes are also expressed to China Construction Third Engineering Bureau Group Co., Ltd. for providing partial financial supports and HS bolts. Besides, many thanks are delivered to Engineering Structure Laboratory of Tsinghua University for offering technical assistances in conducting tensile tests. Any standpoints, insights, findings and conclusions elaborated in this paper are those of the authors and do not necessarily reflect the viewpoints of sponsors.

References

[1] Lin X, Yam M, Song Y, Chung K, et al. Net section tension capacity of high strength steel single shear bolted connections. Thin-Walled Struct 2024; 195: 111371.

[2] Zhang Y, Wang J, Gao S, Wang S, FU F. Tensile resistance of bolted angle connections in the beam-column joint against progressive collapse. Eng Struct 2021; 236: 112106.

[3] Zhang Y, Gao S, Guo L, Qu J, Wang S. Ultimate tensile behavior of bolted T-stub connections with preload. J Build Eng 2022; 47: 103833.

[4] Zhang Y, Gao S, Du E, Fang Y. Ultimate tensile properties of bolted stiffened angle connections. Structures 2023; 55: 2370-2388.

[5] Debnath P, Chan T. Tensile behaviour of headed anchored hollo-bolts in concrete filled hollow steel tube connections. Eng Struct 2021; 234: 111982.

[6] Qiang X, Duan X, Jiang X, Lu Q, Zhou G. Experimental study on mechanical properties of bolted joints between Fe-SMA and steel plates. Eng Struct 2023; 297: 116980.

[7] Zhang Y, Yang F, Sun Y, Zhou Q, Liu Y. Steel shear behaviour on bearing strength and failure modes of single-bolt connections. J Constr Steel Res 2023; 205: 107881.

[8] Wang Y, Jiang Y, Huang Z, Li L, Huang Y, Zhang Y, etc. Study on shear behavior of super-tightened high-strength bolted group connections. J Build Eng 2023; 76: 107308.

[9] Zhu Y, Zhang X, Kong W, Chen Y, et al. Experimental and numerical investigations on shear behavior of high-strength bolted connections after impact. J Build Eng 2023; 79: 107872.

[10] Gong Y. Ultimate tensile deformation and strength capacities of bolted-angle connections. J Constr Steel Res 2014; 100: 50-59.

[11] Li J, Xin H, Wang Z, Veljkovic M, et al. Numerical parametric evaluation of ultimate resistance of high-strength bolts. Structures 2023; 56: 104967.

[12] Milone A, Foti P, Viespoli L, Wan D, et al. Influence of hot-dip galvanization on the fatigue performance of high-strength bolted connections. Eng Struct 2024; 299: 117136.

[13] Guo Q, Zhao Z, Lu Y, Xing Y, et al. Corrosion evolution and axial mechanical performance degradation of corroded M24 high-strength bolts. J Constr Steel Res 2024; 213: 108411.

[14] Chen D, Qu H, Li W, Huang A, et al. Shear performance of high-strength bolted connections with stainless-clad steel plates in a corrosive environment. Thin-Walled Struct 2024; 199: 111770.

[15] Lian F, Zhao B, Li T, Jin Z, Zhao Z. Shear capacity of corroded high-strength bolted connections. Int J Pres Ves Pip 2023; 204: 104981.

[16]Kim I, Lee J, Huh J, Ahn J. Tensile behaviors of friction bolt connection with bolt head corrosion damage: Experimental research B. Eng Fail Anal 2016; 59: 526-543.

[17] Gao S, Li J, Guo L, Bai Q, Li F. Mechanical properties and low-temperature impact toughness of high-strength bolts after elevated temperatures. J Build Eng 2022; 57: 104851.

[18] Zhang T, Bu Y, Wang Y, Chen Z, et al. Experimental study on mechanical properties and tightening method of stainless steel high-strength bolts. Eng Struct 2023; 290: 116176.

[19] Shi G, Shi Y, Wang Y, Bradford M. Numerical simulation of steel pretensioned bolted end-plate connections of different types and details. Eng Struct 2008; 30: 2677-2686.

[20] Yang K, Bai Y, Ding C. Loss of preload of unprotected bolted joints considering environmental effects: A comparative study. J Constr Steel Res 2023; 211: 108211.

[21] Kong Q, Li Y, Wang S, Yuan C, Sang X. The influence of high-strength bolt preload loss on structural mechanical properties. Eng Struct 2022; 271: 114955.

[22] Ban H, Yang Q, Shi Y, Luo Z. Constitutive model of high-performance bolts at elevated temperatures. Eng Struct 2021; 233: 111889.

[23] Yang J, Nie S, Liu M, Huang Y, et al. Constitutive model of austenitic high-strength A4L-80 bolts at elevated temperatures. J Constr Steel Res 2024; 213: 108419.

[24] Liu Y, Jiang J, Chen Q, Cai W, et al. Fracture behavior of Grade 10.9 high-strength bolts and T-stub connections in fire. J Constr Steel Res 2022; 199: 107618.

[25] Meng L, Tu C, Shi Y, Wu Y. Experimental study on shear performance of high-strength bolted connnections fabricated from high-performance fire-resistant steel at elevated temperature. J Build Struct 2021; 42(6): 85-93. (in Chinese)

[26] Kodur V, Yahyai M, Rezaeian A, Eslami M, et al. Residual mechanical properties of high strength steel bolts subjected to heating-cooling cycle. J Constr Steel Res 2017; 131: 122-131.

[27] Mamazizi A, Ahmadi A, Khayati S, Soltanabadi R. Experimental study on post-fire mechanical properties of Grade 12.9 high-strength bolts. Constr Build Mater 2023; 383: 131236.

[28] Ketabdari H, Daryan A, Hassani N. Predicting post-fire mechanical properties of grade 8.8 and 10.9 steel bolts. J Constr Steel Res 2019; 162: 105735.

[29] Firanm M, Ghazijahani T, Cheung J, Mensinger M. Experiments on fire-protected and hot-dip galvanised steel bolted connections. Fire Saf J 2024. (Journal pre-proof)

[30] GB/T 3077-2015. Alloy structure steels. Beijing: China Standards Press; 2016. (in Chinese)

[31] GB/T 2975-2018. Steel and steel products — Location and preparation of samples and test pieces for mechanical testing. Beijing: China Standards Press; 2018. (in Chinese)

[32] GB/T 5267.3-2008. Fasteners — Hot-dip galvanized coatings. Beijing: China Standards Press; 2008. (in Chinese)

[33] GB/T 228.1-2021. Metallic materials — Tensile testing — Part 1: Part 1: Method of test at room temperature. Beijing: China Standards Press; 2021. (in Chinese)

[34] ISO 6892-1: 2016(E). Metallic materials — Tensile testing — Part 1: Method of test at room temperature. Geneva, 2016.

[35] GB/T 3098.1-2010. Mechanical properties of fasteners — Bolts, screws and studs. Beijing: China Standards Press; 2011. (in Chinese)

[36] GB 50017-2017. Standard for design of steel structures. Beijing: China Architecture & Building Press; 2018. (in Chinese)

[37] JGJ 82-2011. Technical specification for high strength bolt connections of steel structues. Beijing: China Architecture & Building Press; 2011. (in Chinese).

[38] Ramberg W, Osgood W R. Description of stress-strain curves by three parameters. Washington: NACA, TN 902; 1943.

[39] Rasmussen K J R. Full-range stress-strain curves for stainless steel alloys. J of Constr Steel Res 2003; 59: 47-61.

[40] Shi G, Zhu X. Study on constitutive model of high-strength structural steel under monotonic loading. Eng Mech 2017; 34(2): 50-59. (in Chinese)S. Adriaenssens, P. Block, D. Veenendaal and C. Williams (eds.), Shell Structures for Architecture: Form Finding and Optimization, Routledge, 2014.